*Tunnelling into a Sustainable Future – Methods and Technologies – Johansson et al (Eds)*
*© 2025 The Author(s), ISBN 978-1-032-90462-7*
*Open Access: www.taylorfrancis.com, CC BY-NC-ND 4.0 license*

# Slope movements monitoring by satellite radar interferometry in the excavation of the Mont Cenis Base Tunnel

M.E. Parisi & M. Calorio
*Engineering Department, Tunnel Euralpin Lyon Turin (Telt) S.a.s., Collegno, Italy*

E. Hugot
*Freelance Geologist, Chambéry, France*

M. Giacoia
*Affari generali per la sostenibilità, l'ambiente e la sicurezza sul lavoro, Department, Tunnel Euralpin Lyon Turin (Telt) S.a.s., Collegno, Italy*

S. Bianchini, M. Del Soldato & N. Casagli
*Department of Earth Sciences - University of Florence, Italy*
*National Institute of Oceanography and Applied Geophysics – OGS, Trieste, Italy*

R. Franceschini
*National Institute of Oceanography and Applied Geophysics – OGS, Trieste, Italy*

M.S. Dahanayaka
*Department of Earth Sciences - University of Florence, Italy*

ABSTRACT: Multi-temporal satellite radar interferometry is based on the analysis of long series of SAR (Synthetic Aperture Radar) images acquired from a satellite platform over the same area at different times. The multiple time intervals permit to perform a back-analysis and a reconstruction of both historical and recent deformation scenarios. A first screening of the past deformations over the area of the Lyon-Turin railway line was carried out through the interferometric analysis of satellite radar data derived from images acquired by Sentinel-1 and COSMO-SkyMed sensors from October 2012 to October 2022. Results of the historical study are presented and cross-compared with ground measurements. Overall, these outcomes provided a complete overview of the deformation scenario of the areas and TELT decided to equip itself with this technology to monitor the slopes during the construction phase.

## 1 INTRODUCTION

The new Lyon-Turin line railway line includes the cross-border section which will be built by TELT. It stretches for 65 km from Saint-Jean-de-Maurienne in France to Susa/Bussoleno (Turin) in Italy. Besides passing the soles, the line crosses the Italian and French Alps with its main work, the 57.5-km-long, twin-tube single-track Mont Cenis Base Tunnel, and connect then to the existing Italian line through the 2-km-long twin-tube single-track interconnection tunnel (Figure 1).

The line, from West to East also includes three adits and one exploratory tunnel already excavated:

- The 2,400-m-long Saint-Martin-la-Porte adit, in France;

DOI: 10.1201/9781003559047-516

- The 2,480-m-long La Praz adit in France;
- The 4,050-m-longVillarodin-Bourget /Modane adit, in France;
- The 7,020-m-long La Maddalena exploratory tunnel with 18 interchange niches, in Italy.

9 km of the south tube of the Mont Cenis Tunnel between Saint-Martin-la-Porte and La Praz, have already been excavated. Four ventilation shafts are under construction.

This complex work includes three underground safety areas with a lot of other smaller works that are useful to the main work and the Saint-Jean-de-Maurienne and Susa international railway stations.

The Mont Cenis Tunnel crosses the main geological units of the Western Alps and the major tectonic contacts, the groundcover overlying the work is particularly high, up to over 2,000 m at the Ambin massif. Due to the complexity of the sectors and on the basis of the historical analysis conducted on the entire area concerned by the cross-border section, at this important stage of the construction of the work, TELT decided to monitor the underground work from above, using the satellite radar interferometry.

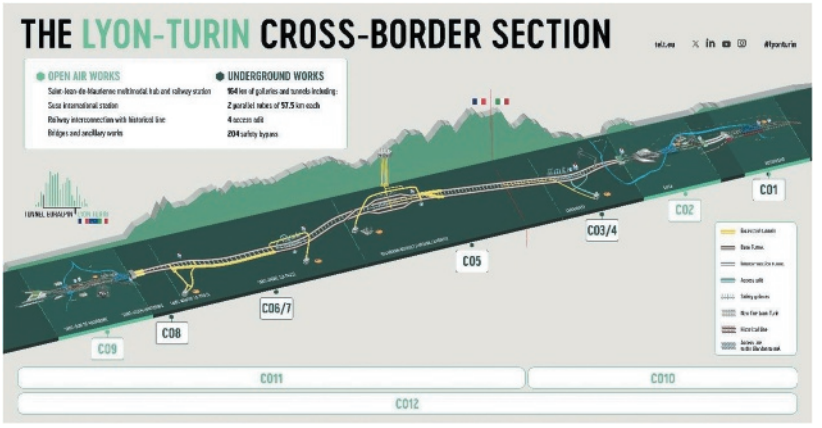


Figure 1. Mont cenis base tunnel of the Lyon-Turin cross-border section.

## 2 GEOLOGICAL SETTING OF THE AREA

### 2.1 *Study area*

The Mont Cenis Tunnel layout crosses an extremely complex geological context, both in terms of lithological variety and in geological-structural terms. The area involves the Western Alps and the Pennine Front which separates the Outer Alps to the West from the Inner Alps to the East (Figure 2).

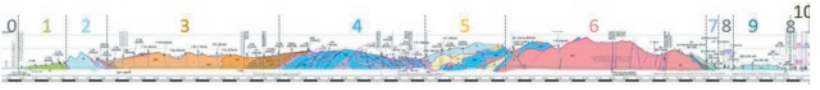


Figure 2. Geological units of the mont cenis tunnel and the interconnection tunnel.

Starting from the west, the Saint Jean de Maurienne portal is built in the alluvial deposits and in the Saint-Julien-Mont-Denis alluvial cone (0). From there, the tunnel crosses the flysch of the Ultradelfinese Zone (1) and once it has crossed the Pennine Front, the tunnel continues into the Sub-briaçonnais Zone (2) whose main lithologies are limestone, dolomite and anhydrite; after crossing the Houiller Front, the tunnel meets the schistose-arenaceous units of the Houiller Brianzonese Sector (3). Then, there is the internal Brianzonese Zone of the Vanoise (4) consisting of mica schists, limestones, dolomites and anhydrites followed by the Schistes

Lustrés stratum on the Gypsum Nappe (5), represented by carbonate rocks and anhydrites. Then, there is the internal Brianzonese Zone of the Ambin massif (6) composed by mica schists and gneisses. In the following metres, the tunnel enters the Tectonic Flake Zone (7), which constitutes a break-off horizon between the Ambin massif and the Piedmont Zone. The Tectonic Flake Zone is characterised by phylladic limestones, albitic and/or chloritic gneisses and tectonic breccias. Then, the Base Tunnel crosses the loose alluvial deposits of the Cenischia torrent sole (0).

This is followed by the Piedmont Zone (9) with calcschists and Charbonnel gneiss, in contact with ultrabasic rocks. The above ground section in the Susa Plain (0) will be built on alluvial deposits. Finally, the Interconnection Tunnel will pass through the phyllosilicate-rich calcschists of the Dora Maira Massif (10).

### 2.2 *Geomorphological background*

As part of the preparatory studies for the construction of the new railway line, geomorphological studies were carried out to assess the geomorphological hazard. These studies allowed to map the phenomena insisting on the areas, among which the dominant slope activities are landslides with prevailing collapse mechanism and deep gravitational slope deformation.

### 2.3 *Cartographic and thematic data*

The area of interest covers approximately 1,000 km2 and was analysed with satellite data from the European Sentinel-1 constellation and the Italian COSMO-SkyMed (Constellation of small Satellites for Mediterranean basin Observation, CSK) constellation, which acquire medium- and high-resolution images in ascending and descending geometry along the satellite's LOS (Line Of Sight).

A multi-layered map base represented by themes such as geology and geomorphology was constructed to contextualise the interpretation of the interferometric data.

The Digital Elevation Model (DEM) with a spatial resolution of 25X25 m, retrieved from the Copernicus portal, was also used. From this data, a slope map was created (Figure 3) with the scale in degrees.

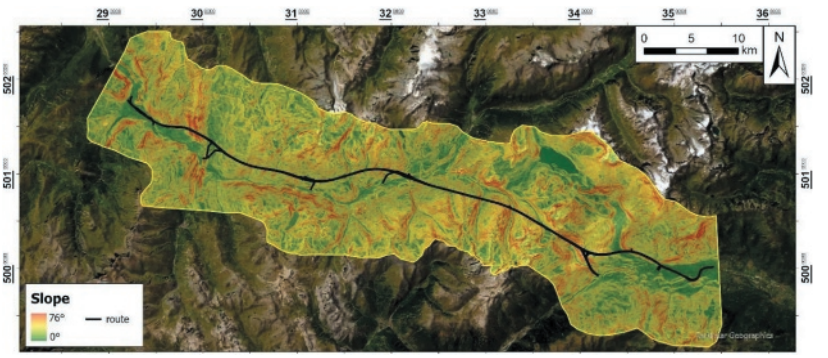


Figure 3. Slope representation.

## 3 METHODOLOGY AND DATA

### 3.1 *Satellite Radar interferometric approach*

Radar techniques are active remote sensing methods: the sensors on board satellites emit microwave radiations to scan targets and areas, and record the backscattering radiation (Bardi et al., 2014). All satellites equipped with SAR (Synthetic Aperture Radar) sensors orbit the Earth on

near-polar orbits from south towards north (in ascending orbit) and from north towards south (in descending orbit) with a lateral right-side line of sight (LOS). SAR images obtained by satellite sensors include amplitude and phase information. The phase information from SAR images can be exploited by using the InSAR (Interferometric Synthetic Aperture Radar) approach, which (Rosen et al., 2000) uses two or more acquisitions of SAR images on the same area over time and allows detecting movements along the sensor (Crosetto et al., 2005) (Figure 4a). The PSI (Persistent Scatterer Interferometry) approach is an advanced InSAR technique that overcomes decorrelation limitations by analyzing a long stack of interferograms and tracking the phase history of stable backscattering points, known as Persistent Scatterers (PS).In this study, SAR images were processed by means of the SqueeSAR algorithm (Ferretti et al. 2011), a multitemporal interferometric processing technique, by relaying on traditional PS and on Distributed Scatterers (DS), homogeneous areas spread over a group of pixels in a SAR image such as rangeland, pasture, shrubs and bare soil. These targets do not produce the same high signal-to-noise ratios of PS, but nonetheless, define an increase of density of the point, especially in natural and non-urban areas (Raspini et al. 2013; Bianchini et al., 2015; Sakkas et al. 2014).

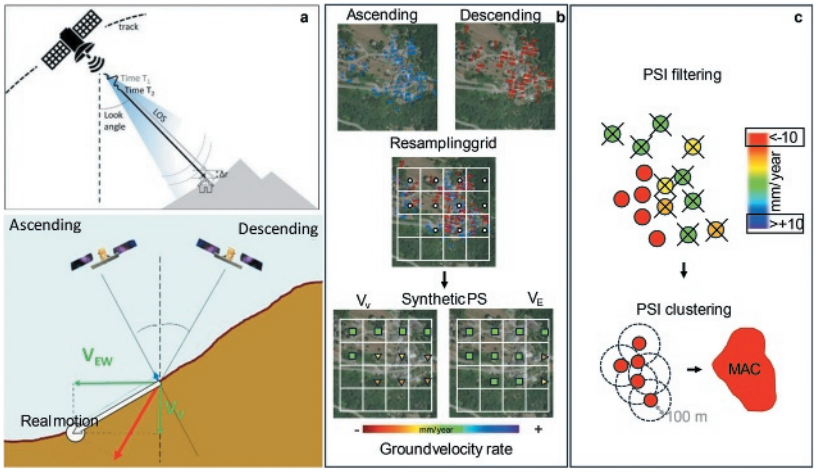


Figure 4. Satellite SAR acquisition and PSI approach (a), scheme of the decomposition of data in vertical and horizontal (b), filtering procedure for obtaining MAC (Moving Active Cluster) areas (c). LOS = satellite Line of Sight; Δr =phase variation.

### 3.2 *Available datasets*

A long series of SAR images acquired in recent time intervals by Sentinel-1 (SNT-1) and COSMO-SkyMed (CSK) missions were considered. The CSK system consists of an ASI (Italian Space Agency) constellation, originally composed by four satellites (Table 1). Sentinel-1 constellation launched by ESA (European Space Agency) within Copernicus program and originally composed of two satellites, Sentinel-1A and Sentinel-1B (Table 1). Overall, 655 SAR images were acquired by SNT-1 satellite in ascending orbit in the period 15/01/2015 - 29/10/2022 and in descending orbit in the period 01/04/2015 - 21/10/2022; a total of 1191 SAR images were acquired by CSK constellation in Stripmap mode, in ascending and descending modes from 22/10/2012 – 26/10/2022.

### 3.3 *Radar-interpretation procedures*

PSI techniques are valuable for detecting slope instability and mapping slow-moving landslides (Meisina et al., 2008; Bianchini et al., 2012) over large areas. The operative methodology of this study over the area of excavation of the Mont Cenis Base Tunnel consisted of four phases:

Table 1. Main characteristics of the used SAR datasets in ascending (Asc.) and descending (Desc.) pass.

| | Sentinel-1 (SNT-1) | | COSMO-SkyMed (CSK) | |
|---|---|---|---|---|
| Satellite | Asc. | Desc. | Asc. | Desc. |
| Microwave band | C | | X | |
| Revisiting time | 12 days | | 16 days | |
| Spatial resolution | 5x20 m | | 3x3 m | |
| Precision in North | ± 2 m | | ± 1 m | |
| Precision in East | ± 6 m | | ± 4 m | |
| Number of images | 323 | 332 | 479 | 712 |
| Track angle | 8.9° | 12.0° | 9.2° | 12.5° |
| Incidence angle | 35.2° | 41.5° | 2,5° | 32,6° |
| Time interval | 01/2015-10/2022 | | 10/2012-10/2022 | |

(i) analysis of LOS mean velocity rates and time series of all available PSI datasets. MP displacement Time Series (TS) show the measured displacement, with millimetre (mm) precision;

(ii) derivation of the East-West and vertical velocity components. Ascending and descending datasets of each sensor were combined to calculate the vertical and horizontal components of the motions by following procedures available in scientific literature (Notti et al., 2014; Bianchini et al., 2014). A spatial sampling grid of 40x40m cell size was used to derive pseudo-targets (Synthetic PS) positioned in the center of the decomposition cell (Figure 4b).

(iii) hotspot analysis through PSI clustering tool. To highlight just the areas characterized by the highest ground motion rates, a hotspot mapping approach recently proposed by Festa et al. (2022) was exploited. The procedure consists in automatically performing a filtering based on a velocity threshold (10 mm/year) and a spatial clustering (100 meters around each PS), considering a minimum number of 3 PS within the maximum 100m distance, and deriving active ground deformation areas called MAC (Moving Area Clusters) (Festa et al. 2022) (Figure 4c).

(iv) cross-comparison with *in-situ* instrumental data and field campaigns. MP data and MAC clusters were compared with available conventional data. In addition, some areas were also the target of field investigations to validate satellite data, verify and better explain the mechanisms generating the remotely sensed measured displacements.

## 4 RESULTS

### 4.1 *Ground deformation maps*

The first result was the ground deformation maps in Sentinel (Figure 5a-b) and CSK (Figure 5c-d). The MP are classified according to the mean annual velocity (expressed in mm/year). Green targets indicate stable or negligible movement (±2.0 mm/year), within the sensitivity range of the interferometric technique. This velocity range is based on dataset standard deviation and in agreement with stable thresholds accepted by the scientific community. Hot colors (negative LOS velocities) indicate movement away from the satellite, while cold colors (positive LOS velocities) indicate movement towards the satellite. Several areas show consistent deformation in both constellations The CSK data shows a not complete coverage of data due to the lack of CSK images acquisition. Another result is the horizontal (Figure 6a) and vertical (Figure 6b) component map, confirming the hypothesis that almost all the ground deformation recorded are related to land instability.

### 4.2 *Case study areas*

The historical analysis of deformations using InSAR data has been conducted on specific areas of interest along the railway route which are characterized by the presence of small settlements and landslide areas.

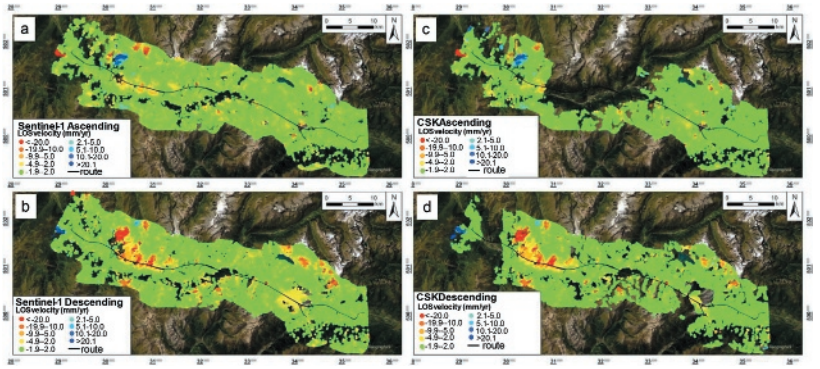


Figure 5. Ground deformation maps of both ascending (a-c) and descending (b-d) geometries, derived from Sentinel-1 and CSK images.

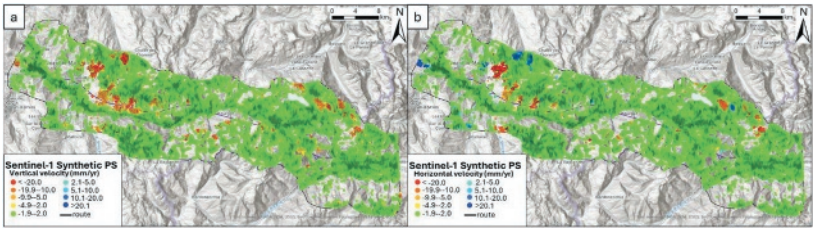


Figure 6. Component deformation maps of vertical (a) and horizontal E-W (b) components.

#### 4.2.1 *The village*

A village near the railway route and its surrounding area were analyzed due to significant velocities and deformation trends indicated by SNT-1 (Figure 7a-b). The village is situated on an extended landslide body (Figure 7d). Located within a MAC zone of active deformation in ascending orbit, the area also had ground leveling survey results available, enabling detailed analysis and on-site data. From the leveling database, DBC3 and DCE6 were selected.

The leveling points were correlated with the time series of the nearest PS point (Figure 8).

Measurement point DBC3, located west of the village, displayed a subsidence trend in the ascending Sentinel-1 data (Figure 8a) with a cumulative displacement of -40 mm. No correlations with descending data were found due to the different LOS direction with respect to the ascending orbit and tow visibility in descending acquisition geometry given the morphological features and exposure of the slope. Point DCE6, within the settlement, is in an active deformation area. In Figure 8b Sentinel-1 data shows a stationary trend from 2014 to 2016, followed by acceleration from 2016 to 2019, and stabilization from 2019 to 2022. Finally, the vertical component (Figure 8c-d) aligns with the trends in the ascending orbit. During the field inspection of the area, changes in slope and irregular hillside morphology were detected, characterized by numerous landslide scarps and counter-slopes.

## 5 DISCUSSION

Although the historical analysis allowed the reconstruction of the deformation scenario of the area where the route of the Turin-Lyon rail tunnel runs, it revealed the advantages of applying this technique but also some limitations.

The main limitations are connected to the intrinsic drawbacks of the PSI techniques that can investigate only slow-moving displacements and that can measure only the component of the

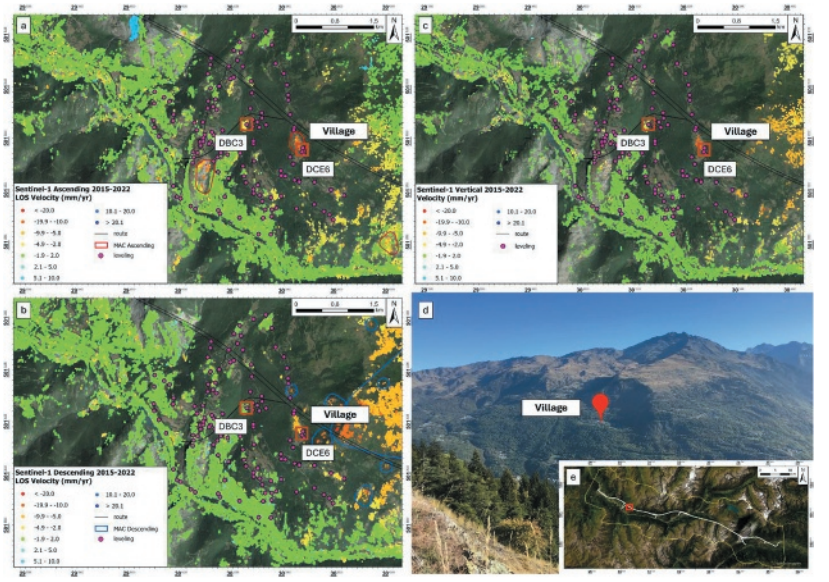


Figure 7. Deformation maps of SNT-1 in ascending (a) and descending (b) orbits with MAClusters, and vertical (c) component. The location of the analyzed PS data and the corresponding leveling point are given by numbering and square, respectively. In (d) and (e) the localization of village.

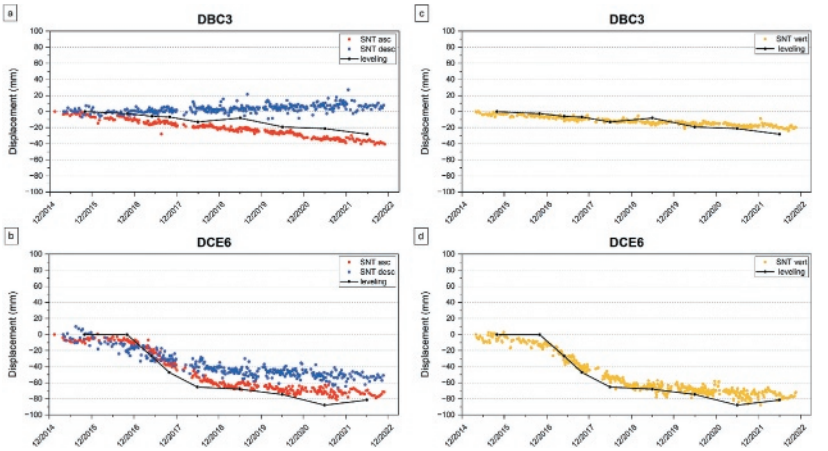


Figure 8. Comparison between time series of the ascending and descending geometries (a-b) and vertical component (c-d) of Sentinel-1 and leveling measurements.

movement along the LOS, which may not fully represent the actual ground motion. Moreover, results can be affected by dense vegetation or changes in surface cover, reducing data reliability in such areas, and by atmospheric conditions like moisture and ionospheric disturbances which can reduce data accuracy. Finally, it is worth to highlight that PSI is not a stand-alone technique, but it requires ground-based validation and further for in-depth investigations.

The main advantages of using PSI SAR data for monitoring slopes are the possibility to measure ground displacements with millimetric accuracy and frequent sampling, the ability to perform back analysis from 1992 up to nowadays, and the benefit of screening deformations over very extensive areas, even at regional-scale.

## 6 CONCLUSIONS

An initial reconstruction of the previous deformation scenario of the area concerned by the Lyon-Turin railway was carried out through the analysis of interferometric satellite radar data derived from images acquired by the Sentinel-1 and COSMO-SkyMed sensors in the period from October 2012 to October 2022.

These satellite radar data was used in a combined way to obtain a more robust, effective and versatile Earth surface observation system. In fact, on the one hand, the use of Sentinel-1 images allows to obtain a complete representation, thanks to the plan of regular acquisitions over a vast area; on the other hand, COSMO-SkyMed acquisitions guarantee the detail needed for high-definition local analyses, thanks to the better spatial resolution compared to Sentinel-1.

The construction of the Mont Cenis Tunnel is in full swing and, on the basis of the experience gained from the historical analysis carried out using satellite interferometry, and in order to obtain an increasingly complete picture of the deformation scenario in the area by monitoring the slopes and the overlying infrastructure, it has been decided to continue the activities by adopting a periodic deformation monitoring service through the processing of data updated on a quarterly basis, using the C-band as the reference analysis band. This technique will accompany the more classic ones such as ground levelling and GPS measurements and, together with other types of monitoring, such as water resource monitoring, will make it possible to monitor the areas concerned by the construction of the new railway link.

## REFERENCES


Bardi, F., Frodella, W., Ciampalini, A., Bianchini, S., Del Ventisette, C., Gigli, G., … & Casagli, N. (2014). Integration between ground based and satellite SAR data in landslide mapping: The San Fratello case study. *Geomorphology*, *223*, 45–60.

Bianchini, S., Cigna, F., Righini, G., Proietti, C., & Casagli, N. (2012). Landslide hotspot mapping by means of persistent scatterer interferometry. *Environmental Earth Sciences*, *67*, 1155–1172.

Bianchini, S., Pratesi, F., Nolesini, T., & Casagli, N. (2015). Building deformation assessment by means of persistent scatterer interferometry analysis on a landslide-affected area: the Volterra (Italy) case study. *Remote sensing*, *7*(4), 4678–4701.

Crosetto, M., Crippa, B., & Biescas, E. (2005). Early detection and in-depth analysis of deformation phenomena by radar interferometry. *Engineering geology*, *79*(1-2), 81–91.

Ferretti, A., Fumagalli, A., Novali, F., Prati, C., Rocca, F., & Rucci, A. (2011). A new algorithm for processing interferometric data-stacks: SqueeSAR. *IEEE transactions on geoscience and remote sensing*, *49*(9), 3460–3470.

Festa, D., Bonano, M., Casagli, N., Confuorto, P., De Luca, C., Del Soldato, M., … & Casu, F. (2022). Nation-wide mapping and classification of ground deformation phenomena through the spatial clustering of P-SBAS InSAR measurements: Italy case study. *ISPRS Journal of Photogrammetry and Remote Sensing*, *189*, 1–22.

Meisina, C., Zucca, F., Notti, D., Colombo, A., Cucchi A, A., Savio, G., … & Bianchi, M. (2008). The use of PSInSAR™ data in landslide detection and monitoring: The example of the Piemonte region (Northern Italy). In *Proceedings of the Tenth International Symposium on Landslides and Engineered Slopes (Volume 2)*.

Raspini, F., Moretti, S., & Casagli, N. (2013). Landslide mapping using SqueeSAR data: Giampilieri (Italy) case study. *Landslide Science and Practice: Volume 1: Landslide Inventory and Susceptibility and Hazard Zoning*, 147–154.

Rosen, P. A., Hensley, S., Joughin, I. R., Li, F. K., Madsen, S. N., Rodriguez, E., & Goldstein, R. M. (2000). Synthetic aperture radar interferometry. *Proceedings of the IEEE*, *88*(3), 333–382.

Sakkas, V., Novali, F., Lagios, E., Bellotti, F., Vassilopoulou, S., Damiata, B. N., & Allievi, J. (2014, July). Ground deformation study of KOS island (SE Greece) based on Squee-SAR™ interferometric technique. In *2014 IEEE Geoscience and Remote Sensing Symposium* (pp. 4319–4322). IEEE.